Optik - International Journal for Light and Electron Optics xxx (xxxx) xxxx

Contents lists available at ScienceDirect

Optik

journal homepage: www.elsevier.com/locate/ijleo

Original research article

Study of space optical dynamic push-broom imaging along the trace of targets

Chao Xu[a,b], Xiubin Yang[a,*], Tingting Xu[a,b], Lin Zhu[a,b], Lin Chang[a], Guang Jin[a], Xiangdong Qi[a]

[a] Changchun Institute of Optics, Fine Mechanics and Physics, Chinese Academy of Science, Changchun, Jilin code130033,China
[b] University of Chinese Academy of Science, Beijing code100049, China

ARTICLE INFO

Keywords:
Dynamic push-broom imaging
TDI camera
Satellite attitude
temporal resolution
velocity mapping

ABSTRACT

In order to scan efficiently along the trace of curve-distributed off-track targets, a novel push-broom imaging method is proposed. Firstly, the trace equation is fitted to optimize the number of detectable targets. To achieve the shortest attitude maneuver time, the triaxial attitude of the satellite is solved in real time, and the TDI imaging velocity is made consistent with the direction of the trace. Finally, the ground imaging simulation is performed, and JL-1 Smart Verification Satellite is utilized to verify that the imaging temporal resolution has been improved by more than 4 times.

1. Introduction

At present, traditional Earth observation satellites(EOSs) mostly adopt sun-synchronous orbit, and can only perform push-broom imaging, which scans along the satellite orbit with a relatively low imaging efficiency [1]. Usually, this scanning method works well when the targets are distributed along the ground track. However, when it comes to the curve-distributed targets, it is hardly possible to get a full coverage surveillance of them with a single scan. Here the curve-distributed targets are characterized by some discrete or continuous ground scenes, whose overall distribution is not straight but always in curved shape geometrically, for instance, rivers, metropolitan stretches, or international boundary. Therefore, multiple revisiting scan will be required. Considering the revisit period of the EOSs, the scanning time will be greatly increased, and the imaging efficiency will be reduced [2]. In addition, if the targets are highly time-variable, the accuracy of imaging will deteriorate further [3]. Usually, this problem can be alleviated by strengthening the attitude maneuverability of EOSs. For a target which is deviated from the satellite ground track, the satellite bus must roll itself to aim at it. For the curve-distributed targets, the roll angles are not the same, and the satellite must switch its attitude between different targets. This process depends heavily on the attitude maneuverability of the satellite. However, the modification of the satellite platforms will greatly increase the manufacturing cost.

In order to improve the observation efficiency and accuracy of EOSs without changing the hardware of the satellite, a series of research have been done. Xu et al.[4] proposed a total priori value maximization model for satellite imaging scheduling. The targets of curved distribution are divided into multiple satellite imaging tasks, and each task represents a certain prior value. In order to maximize imaging efficiency, it is necessary to maximize the total a priori value. Tangpattanakula et al.[5] proposed a multi-object local search model from the perspective of users, ensuring that the effective information of the imaging area is maximized, and the

* Corresponding author at: Dongnanhu Road, 3888, Changchun, Jilin, China.
E-mail addresses: 3130102190@zju.edu.cn (C. Xu), yangxiubin@ciomp.ac.cn (X. Yang), 1422168015@qq.com (T. Xu), zhul370@163.com (L. Zhu), fanlinchang@aliyun.com (L. Chang), jing@ciomp.ac.cn (G. Jin), chinagrating@263.net (X. Qi).

https://doi.org/10.1016/j.ijleo.2019.163640
Received 3 August 2019; Accepted 13 October 2019

difference of information obtained by each user is minimized. Since the scheduling of imaging satellites was proved to be NP-hard [6], it was solved mainly by heuristic algorithm [7] or meta-heuristics such as genetic algorithm [8]. Li et al.[9] proposed an idea that decomposed the scheduling problem into task assignment main problem and single satellite scheduling sub-problem. Multi-satellites are utilized in the algorithm. An ant colony optimization algorithm was adopted to optimize the task assignment scheme, and a fast simulated annealing algorithm was used to solve the single satellite scheduling problem.

The methods mentioned upfront work well when there are limited number of ground objects. Considering the great amount of targets, such as curve-distributed targets in this paper, the methods mentioned above demand a lot for the optimization algorithm, otherwise, the calculation cost will be dramatically high. Therefore, from the respect of curve-distributed targets, it is actually a new type of problem of scheduling and detection. This paper first proposes a novel targets coverage algorithm, in which a three-dimensional spatial vascular tube is devised to envelop most detectable targets with simple mathematics. This algorithm obtains the three dimensional information of the targets; thus it is able to determine whether the targets pointed by the Time Delay Integral(TDI) camera's boresight are in its field of view. Then, a triaxial attitude model is specially conceived to make the satellite scan along the trace of targets. The Euler quaternion is adopted to extract the optimal attitude angle, so the satellite bus adapts itself with the shortest maneuver path to make the TDI camera's imaging direction consistent with the targets' distribution. The algorithm and the model proposed in this paper are combined as Smart Imaging method. It has been used in JL-1 Smart Verification Satellite, and shows a great performance. The satellite realizes rapid observation of the curve-distributed targets within single revisit period, effectively improving the imaging efficiency and accuracy.

Overall, the contributions of this work are mainly in the following aspects:

1. A coverage algorithm is proposed to determine the most detectable targets with a three-dimensional spatial vascular tube, which is constructed by the swath of TDI camera, the longitude and latitude of the targets.
2. A satellite triaxial attitude model is built to make the TDI camera's imaging direction coincide with the targets' distribution.
3. The proposed Smart Imaging method shows a prospect for on-orbit application of agile satellite, and the imaging efficiency can be greatly increased with quite simple mathematics.

The rest of the paper is arranged as follows: Section 2 presents a mathematical model of the targets planning problem. Section 3 proposes a scheduling algorithm for including the most targets in a 3D spatial vascular tube limited by satellite swath. In Section 4, the optimum maneuvering path of the satellite is designed to solve the three-axis attitude pointing to the curve-distributed targets in real time. Section 5 establishes a ground simulation system and JL-1 Smart Verification Satellite is utilized to verify our Smart Imaging method. In Section 6, a conclusion of this paper and future research work are given.

2. Mathematical model of scheduling problem

The problem in this work is to make the satellite scan along the trace of targets. Firstly, it is necessary to find a proper targets scheduling algorithm to determine most detectable ground scenes. Considering the great number of the curve-distributed targets, simple mathematics are preferred for on-orbit use. Then, the satellite bus adapts its attitude to perform dynamic push-broom imaging along the trace of targets.

For the target scheduling algorithm, a practical mathematical model should be formulated. The decision function is quite obvious,

$$F = \begin{cases} l1, \text{detectable} \\ 0, \text{ undetectable} \end{cases} \tag{1}$$

In our algorithm later proposed, the detectable target means the one which is in the three-dimensional spatial vascular tube, on the other hand, the outliers are the targets out of the tube.

The major constraints to fulfill are related to the orbital height of the satellite, the field of view(FOV) of the TDI camera and the distribution of the targets. Once the satellite is launched, the former two parameters are fixed. Therefore, the distribution of the targets is the main point we concern about.

Based on the practical circumstances of our problem, some assumptions are presented as follows.

1. The targets mentioned in this paper can be either on the ground or near the ground, which is more reasonable in real scenes, for instance, rivers, high-rises, or mountains. However, compared with the radius of Earth or the orbital height of the satellite, the targets' altitude is so trivial that it can be neglected for mathematical simplicity.
2. The attitude model depends on the maneuverability of the satellite, but does not rely heavily on it. The purpose of our method is actually to alleviate the burden on the satellite's maneuverability.
3. From a research perspective, the algorithm should be optimized, for example, the number of detectable targets, varied importance of the targets, and the energy cost of adapting the satellite bus to the desired attitude. However, considering the limited resource of the satellite processor, we tend not to do much optimization on orbit. Instead, the satellite transmits the data back to the ground station, and then the optimum choice will be made.

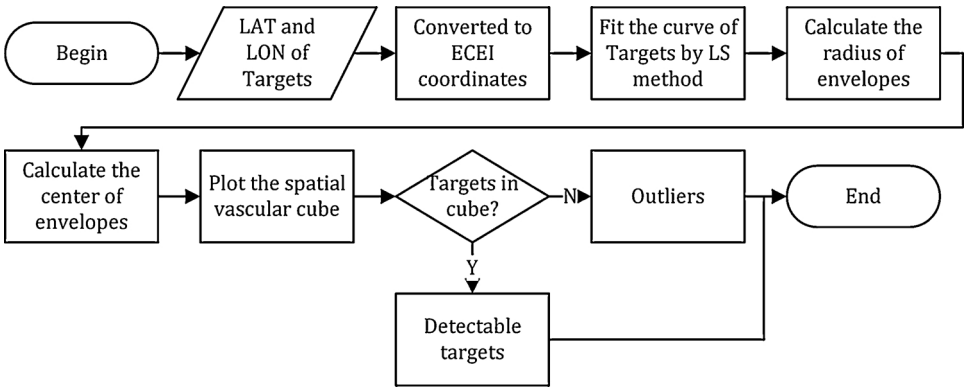

Fig. 1. Flowchart of the proposed targets scheduling algorithm.

3. Proposed targets scheduling algorithm

In this section, we first determine the location of the targets in three-dimensional space according to the latitude and longitude, and use the least squares method to fit the path to obtain the polynomial coefficients. Then the polynomial curve is used as the central axis, and the imaging swath as the chord length. Finally, a spatial vascular tube is constructed to determine the imaging region of the distributed targets. The overall flowchart of our method is shown in Fig. 1.

3.1. Three-dimensional spatial curve fitting of distributed targets

For a series of target points (α_i, δ_i) near the ground surface, and represent the longitude and latitude of the targets, respectively. In order to utilize the swath of satellite, (α_i, δ_i) needs to be converted into Earth-centered Earth-fixed (ECEF) coordinate. The conversion relationship is shown in Fig. 2 and the formulas are as below:

$$\begin{cases} x_i = R\cos\delta_i\cos\alpha_i \\ y_i = R\cos\delta_i\sin\alpha_i \\ z_i = R\sin\delta_i \end{cases} \tag{2}$$

$$\begin{cases} \alpha_i = \arctan(y_i/x_i \\ \delta_i = z_i/\sqrt{x_i^2 + y_i^2} \end{cases} \tag{3}$$

where R is the radius of the earth.

In the ECEF coordinate, the least square method is employed to find the best fitting curve equation of the targets, considering its simple mathematics but great efficiency compared with Radial Basis Function or Spline Fitting method. Assuming a parameter t, the parameter equation of the three-dimensional spatial curve is as follows:

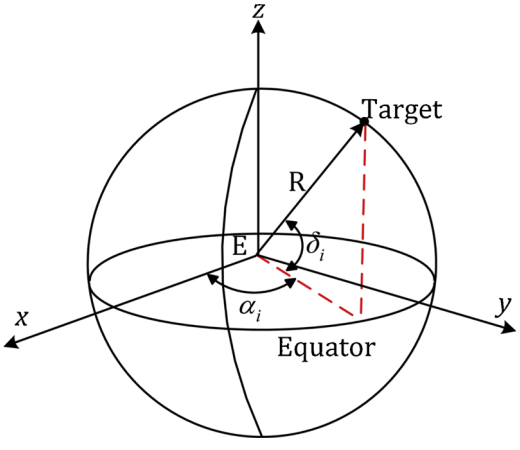

Fig. 2. Coordinate transform diagram.

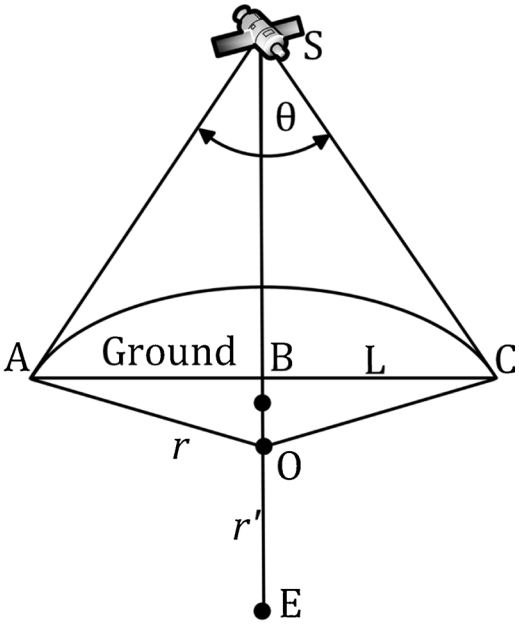

Fig. 3. Cross-section schematic diagram of spatial vascular tube.

$$\begin{cases} cx(t) = A_N \cdot t^N + \cdots A_1 \cdot t + A_0 \\ y(t) = B_N \cdot t^N + \cdots B_1 \cdot t + B_0 \\ z(t) = C_N \cdot t^N + \cdots C_1 \cdot t + C_0 \end{cases} \tag{4}$$

where $A_N, \cdots, A_1, A_0$ are the coefficients of the surface $x = x(t)$; $B_N, \cdots, B_1, B_0$ are the coefficients of the surface $y = y(t)$; $C_N, \cdots, C_1, C_0$ are the coefficients of the surface $z = z(t)$. N denotes the order of the curve equation, which can be altered to obtain an optimal detection of the distributed targets. In practical use, N should be no more than 6, otherwise, it will be difficult for the satellite processor to solve the real-time attitude and the calculation time will be greatly increased.

3.2. Three-dimensional spatial vascular tube drawing limited by swath

After fitting the curve equation of the targets, a three-dimensional vascular tube is constructed to maximize the number of detectable targets. As shown in Fig. 3, the tube is constructed with the targets curve as the central axis and the swath as the chord length of the envelope circle. The circle is tangent to the marginal FOV of the TDI camera. Here O denotes the center of the envelope circle, and r' denotes the distance between O and Earth center E. The radius of the envelope circle is r and the FOV of the TDI camera is θ. L is the swath of the satellite on the earth ground. S represents the position of the satellite at a certain moment. Since the ground is large enough compared with the swath, it is assumed to be plane. S and E are connected to intersect the ground surface at the point B,with its location (α, δ). The coordinates in the ECEF system can be expressed as (x', y', z'). Next, the center O and the radius r of the envelope circle will be derived.

In ΔOAB and ΔASB, $\angle OAB = \angle ASB = \theta/2$, $AB = L/2$, thus the radius r of the envelope circle is calculated as:

$$r = \frac{L}{2\cos(\theta/2)} \tag{5}$$

In ΔOAB, $BO = L/2 \times \tan(\theta/2)$. Therefore, r' is calculated as follows:

$$r' = R - \mathrm{BO} = R - \frac{L}{2}\tan(\frac{\theta}{2}) \tag{6}$$

It can be seen in Fig. 3 that the points S, B, O are collinear, therefore, in the ECEF coordinate system, the coordinates of O can be expressed as:

$$\begin{cases} x_O = [R - L/2 \cdot \tan(\theta/2)]\cos\delta \cdot \cos\alpha \\ y_O = [R - L/2 \cdot \tan(\theta/2)]\cos\delta \cdot \sin\alpha \\ z_O = [R - L/2 \cdot \tan(\theta/2)]\sin\delta \end{cases} \tag{7}$$

When the satellite is in different positions, the positions of B_i are also different, then a series of O_i can be calculated, in which $i = 1, b, \cdots, n$ and n is the number of envelope circles. Finally, taking the points O_i as the center of the circles, r as the radius, a series

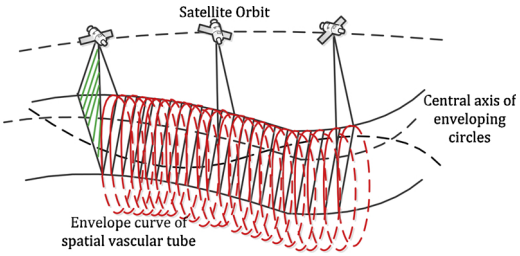

Fig. 4. Spatial diagram of satellite imaging path for targets.

of envelope circles are created to constitute the three-dimensional spatial vascular tube. Overall, the algorithmic computational complexity is $O(n)$.

3.3. Evaluation of three-dimensional spatial vascular tube

The perspective view of a satellite imaging path is shown in Fig. 4 for the curve-distributed targets. Since the FOV of the TDI camera is limited, the effective area actually observed by the satellite can be represented by the red part, and the targets out of the observation range is in green. The shortest distance d from the target point to the center of the corresponding envelope circle is calculated. If the distance d is smaller than the radius of the envelope r, the point is considered detectable by adjusting the satellite's three-axis attitude. Otherwise, the target is considered to be an undetectable outlier. As was mentioned before, different fitting orders of least squares method need to be chosen to maximize the number of detectable target points.

A spatial vascular slice area is selected to specify whether the distributed target is enveloped or not. As shown in Fig. 5, firstly, the targets outside the FOV of the TDI camera cannot be detected. Secondly, since we mainly concern about the targets which are near the ground, the spatial targets below the surface and above the envelope circle are also thought to be undetectable. That is, only the targets in the red area can be detected. For the target point t_1, the distance d_1 from t_1 to the center of the circle O is larger than r, so the target point is rejected. For the point t_2, d_2 is smaller than r, thus t_2 is retained. As a result, the green target points should be eliminated, and the purple ones are the targets that should be retained.

4. Triaxial attitude model of Smart Imaging

After the detectable area is determined, in order to make the scanning direction consistent with the distribution of the targets, the Smart Imaging model is established. When the satellite is approaching the above of the targets, the triaxial attitude angle should be tuned to make the camera boresight point to the targets exactly [10,11]. Fig. 6 shows the process of the satellite adapting its attitude. Firstly, the boresight points to the satellite nadir M, then a pitch angle θ is exerted to make it point to N. Here M and N are on the same longitude line. After that, the satellite bus performs a roll angle φ, and the boresight points to T. Finally, a yaw angle ψ and a roll angular velocity $\dot{\varphi}$ are performed to make the trace parallel to TDI scanning direction. The process mentioned above is also briefly shown in the flowchart of Fig. 7.

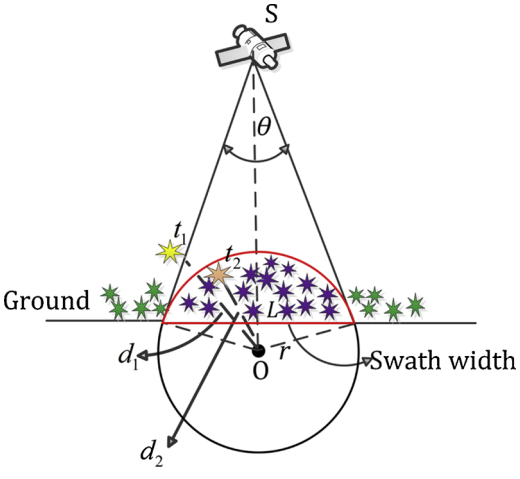

Fig. 5. Cross-section diagram of satellite imaging path for targets.

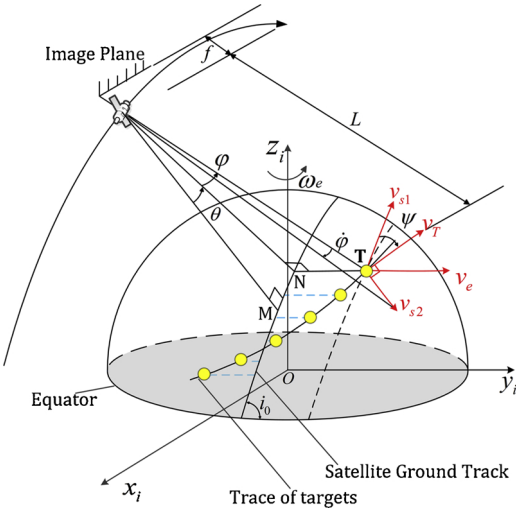

Fig. 6. Process scheme map of Smart Imaging.

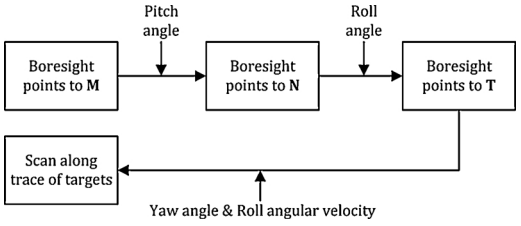

Fig. 7. Flowchart of the satellite adapting its attitude.

4.1. Calculation of roll angle

In practical applications, the pitch angle is set $\theta = 0$, which saves the maneuver energy of the satellite bus. Under this circumstance, N is the sub satellite point. Then, in order to solve the roll attitude angle, some coordinate systems need to be set up [12], including Earth Centered Inertial (ECI) $I(x_i, y_i, z_i)$, satellite body $S(x_s, y_s, z_s)$, and orbital coordinate $O(x_o, y_o, z_o)$, as shown in Fig. 8.

In the traditional pushbroom pattern, since the camera is fixed on the satellite bus, the TDI camera's boresight r_S always points from the satellite to the Earth's center. The satellite's observation vector r_{ST}, on the other hand, is the connection between the satellite and the target. In order to scan along the trace, it is first necessary to make the boresight vector r_S coincides with the satellite's observation vector r_{ST}, which means r_S does not point to the Earth's center but to the target in our case.

The observation target $T(\alpha, \delta)$ in ECI coordinate system is expressed as,

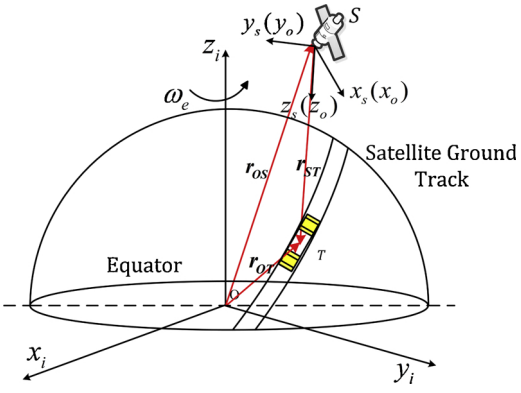

Fig. 8. Schematic diagram of coordinate systems.

$$r_{\mathrm{OT}}^{I}=\begin{bmatrix} cx_{\mathrm{OT}}^{I} \\ y_{\mathrm{OT}}^{I} \\ z_{\mathrm{OT}}^{I} \end{bmatrix}=R\cdot\begin{bmatrix} c\cos\delta\cos\alpha \\ \cos\delta\sin\alpha \\ \sin\delta \end{bmatrix} \tag{8}$$

To transform r_{ST} in the ECI coordinate to r_{ST}^{O} in the orbital coordinate, a coordinate transformation matrix A_I^O is required,

$$A_I^O=R_{\mathrm{Iy}}(-\frac{\pi}{2})R_{\mathrm{Ix}}(-\frac{\pi}{2})R_{\mathrm{Iz}}(\omega+\nu)R_{\mathrm{Ix}}(i_0)R_{\mathrm{Iz}}(\Omega) \tag{9}$$

where ω is the perigee angle, ν is the true anomaly, and i is the orbital inclination. Ω is the right ascension of ascending node. R_I is the standard rotation matrix [13]. Then, r_{ST}^{O} is solved as below,

$$r_{\mathrm{ST}}^{O}=A_I^O(r_{\mathrm{OT}}^{I}-r_{\mathrm{OS}}^{I}) \tag{10}$$

wherein, r_{OT}^{I} and r_{OS}^{I} represent the position vector of the target and the satellite in the ECI coordinate. Similarly, r_{OS}^{O} in the orbital coordinate is obtained from r_{OS}^{I}.

To point at the target, the satellite can choose any maneuver path to the desired attitude. In our case, we expect to get the shortest maneuver path. Therefore, the Euler quaternion Q is referred to obtain the triaxial angles [14]. Here the triaxial angles are defined by the attitude of the satellite body relative to the orbital coordinate system. The initial vector r_{ST}^{O} and r_{OS}^{O} will be the only parameters required to get the quaternion Q, which can be expressed as:

$$Q=\begin{bmatrix} q_1 \\ q_2 \\ q_3 \\ q_4 \end{bmatrix}=\begin{bmatrix} e_x\sin(\phi/2) \\ e_y\sin(\phi/2) \\ e_z\sin(\phi/2) \\ \cos(\phi/2) \end{bmatrix}=\begin{bmatrix} e\sin(\phi/2) \\ \cos(\phi/2) \end{bmatrix} \tag{11}$$

e is the Euler axis, and ϕ is the Euler angle, which are defined as below:

$$e=\frac{r_{\mathrm{OS}}^{O}\times r_{\mathrm{ST}}^{O}}{\|\, r_{\mathrm{OS}}^{O}\times r_{\mathrm{ST}}^{O}\,\|} \tag{12}$$

$$\phi=\arccos\frac{r_{\mathrm{OS}}^{O}\cdot r_{\mathrm{ST}}^{O}}{\|\, r_{\mathrm{OS}}^{O}\,\|\cdot\|\, r_{\mathrm{ST}}^{O}\,\|} \tag{13}$$

After the Euler quaternion is solved, the expected roll angle can be expressed as [14]:

$$\varphi=\arcsin[2(q_2q_3-q_1q_4)] \tag{14}$$

It should be noted that the yaw and pitch angle can also be derived from the Euler quaternion. However, in this case, when the pitch is preset as 0, the yaw angle has infinite solutions. It is easy to consider: the satellite bus can point to the target by adapting its roll angle, after that, no matter how it changes the yaw angle, the boresight of the TDI camera always points to the target. Therefore, in order to scan along the targets, another strategy should be adopted to obtain the yaw angle.

4.2. Calculation of yaw angle and roll angular velocity

After the satellite bus performs the pitch and roll angle, the boresight of the TDI camera exactly points to the target. However, the scanning area for now is still parallel with the satellite round track. In order to make the satellite's sweep direction consistent with the targets distribution, the satellite yaw angle must be precisely adjusted as well as the roll angular velocity [15,16].

As shown in Fig. 6, v_{s1} is the scanning velocity at the target point T after the satellite performs the roll angle φ, v_e is the Earth rotation velocity at T, and v_T is the desired velocity of push-broom imaging along the trace. The yaw angle ψ needs to be adjusted along the targets' trace, and it can be calculated implicitly by the following formula:

$$v_{s1}\cos\psi+v_e\cos(i_0-\psi)=v_T \tag{15}$$

where i_0 is the orbital inclination, v_{s1} and v_e can be expressed as:

$$v_{s1}=\Omega_O\cdot(R+h-L\cos\theta\cos\varphi) \tag{16}$$

$$v_e=\omega_e\cdot R\cdot\cos\delta \tag{17}$$

where Ω_O is the orbital angular velocity, R is the radius of Earth, h is the orbital height, ω_e is the angular velocity of the earth's rotation, and δ is the latitude of the target point. The distance between the optical center of the TDI camera and the target point can be expressed as:

$$L=(R+h)\cdot\cos\theta\cos\varphi-\sqrt{R^2-(R+h)^2\cdot(1-\cos^2\theta\cos^2\varphi)} \tag{18}$$

When the satellite performs the yaw angle ψ, it is also necessary to apply a roll angular velocity $\dot{\varphi}$ perpendicular to the push-broom direction to generate v_{s2} on the ground. Finally, the composite velocity v_T at the target T is consistent with the targets distribution. v_{s2}

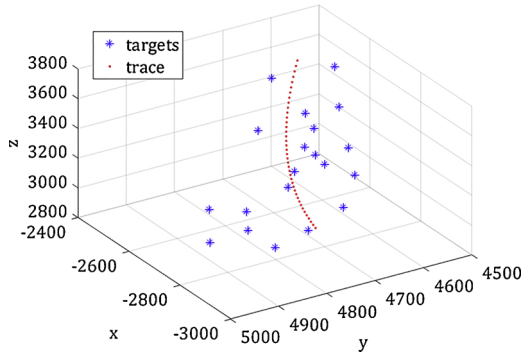

Fig. 9. Distribution of targets fitted by 2nd order least squares method.

can be expressed as:

$$v_{s2} = \dot{\varphi} L \tag{19}$$

Therefore, the roll angular velocity can be solved:

$$\dot{\varphi} = \frac{v_{s1}}{L} \sin\psi - \frac{v_e}{L} \sin(i_0 - \psi) \tag{20}$$

5. Simulation experiments and on-orbit verification of Smart Imaging method

In this section, an example of the Yangtze River Delta is simulated to demonstrate the enveloping algorithm of spatial vascular tube, then ground experiments are carried out to evaluate the theoretical feasibility of Smart Imaging method. Finally, the imaging verification is performed on orbit using JL-1 Smart Verication Satellite.

5.1. Demonstration of spatial vascular tube enveloping targets

This section will model the 20 cities of the Yangtze River Delta, an economically developed region in China. The latitude and longitude coordinates are extracted, and they are converted into the ECEF coordinate system. In this case, the orbital height of the satellite is 650km, and the field of view is 1°. Then the second-order least squares method is chosen to fit the target points and the results are shown in Fig. 9. As was mentioned earlier, in the ECEF coordinate system, the envelope circles are drawn with the points O_i as the centers and r as the radius. A series of envelope circles constitute the three-dimensional spatial vascular tube, and the result is shown in Fig. 10. The trace of the targets is represented by the red dots, and the outliers are marked by the pink squares. As a result, the number of target points that can be detected is 12, with the ratio being 0.6.

In order to select the optimal target scheduling scheme, we set different polynomial orders to view the detection results. For each order, we iterate the algorithm for 1000 times, then the calculation time is recorded as an indicator of computational cost. The simulation is performed on Matlab 2019a, and the running system is Windows 10 with Intel Core i7-7700 CPU and RAM of 32GB. Although the processor of the satellite bus differs from our CPU, the analysis here can still be a reference for finding the optimal fitting order. The results are shown in Table 1.

Considering the computational cost and the detectable ratio, it is more appropriate to use the second-order polynomial for the observation area. The target detectable ratio is 0.6000, and the calculation time is 7.884515s. The ratio of 4th order polynomial is 0.6500 with the calculation time reaching 8.716120s, however, its computational cost is increased by 10.5% compared with the 2nd

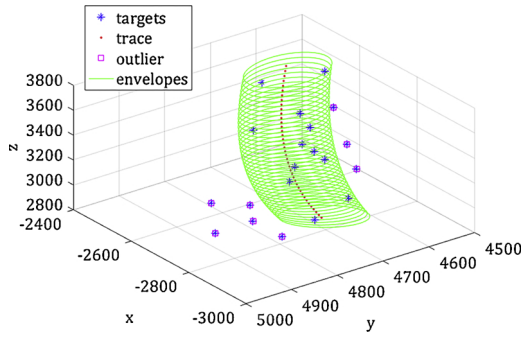

Fig. 10. Envelopes of spatial vascular tube with 2nd order least squares method.

Table 1
Detection results under different fitting order.

Order	Detectable number	Detectable ratio	Calculation time(1000 iterations)/s
1	10	0.5000	7.844640
2	12	0.6000	7.884515
3	12	0.6000	8.001481
4	13	0.6500	8.716120
5	13	0.6500	8.701817
6	12	0.6000	8.719878

polynomial. Note that the processing speed of satellite bus will be much slower since it should take care of other tasks, for instance, deciding the high priority target, or controlling the solar power panels. It turns out that the real-time adjustment of satellite attitude will be much more difficult. We need to make a tradeoff between the detectable ratio and computational cost. In addition, it can also be seen from Table 1 that as the fitting order is higher, the number of detectable targets do not always get larger.

As shown in Fig. 11, for the 20 targets in Yangtze River Delta, using our method, there are 12 detectable points which are represented by the balloons. The result is actually quite thrilling since a normal push-broom pattern can only collect 3 targets, which are represented by the circles in this case. The asterisks are the targets which cannot be detected by either of the methods. Generally speaking, the traditional push-broom scanning is capable of covering the target points distributed along the satellite ground track, as is shown by the rectangular scanning area, but it is greatly limited by the orbital height and FOV of the satellite. Our dynamic push-broom method, instead, is actually not constrained by the problem. As was mentioned above, we maximize the detectable targets and find the optimal maneuver path to make the satellite bus adapt its attitude in the shortest time.

According to Eq.(4)), the distribution function of the detectable points can be obtained as follows:

$$\begin{cases} x(t) = t \\ y(t) = 11.363087t^2 - 36.503525t + 4736.552879 \\ z(t) = 13.254075t^2 + 136.941594t + 3264.566307 \end{cases} \tag{21}$$

Finally, the relationship between the latitude and longitude can be found using Eq.(3), and it is expressed as below:

$$\begin{cases} \alpha = \arctan\left(11.363087t + \dfrac{4736.552879}{t} - 36.503525\right) \\ \delta = \dfrac{13.254075t^2 + 136.941594t + 3264.566307}{\sqrt{t^2 + (11.363087t^2 - 36.503525t + 4736.552879)^2}} \end{cases} \tag{22}$$

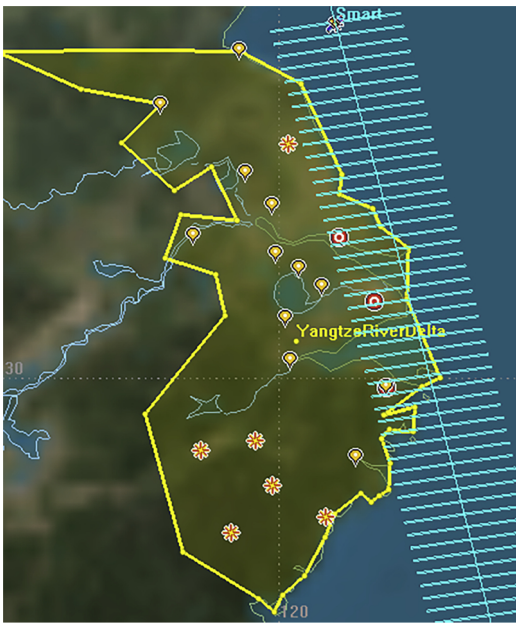

Fig. 11. Detectable area for 20 cities in Yangtze River Delta.

Fig. 12. Simulation experimental equipment of Smart Imaging.

5.2. Ground simulation of Smart Imaging

The imaging simulation equipment is shown in Fig. 12. The satellite attitude-controlling simulation platform is mainly composed of a triaxial air-floating turntable, a TDI camera, and a P4 curved LED screen. The triaxial air-floating turntable can adapt its attitude. The high-resolution TDI camera is fixed on the turntable to simulate Smart Imaging, the pixel size of CCD is 8 m and the focal length of the lens is 8 mm. The P4 curved LED has a size of 6 m × 4 m, a radius of curvature of 32 m, and a pixel size of 4 mm.

As shown in Fig. 13, the triaxial air-floating turntable coordinate system is defined. The z-axis points to the LED screen, the x-axis is perpendicular to the table, and the y-axis forms the right-hand coordinate system with the x and z axes. In the simulation experiment, v_1 is the velocity generated on the LED curved screen by the rotation of the turntable, which matches the rotation velocity of the earth; v_2 is the velocity generated by the movement of the target points, which matches the precession speed of the satellite.

This section virtually sets 8 target points, whose latitude and longitude are shown in Table 2. These targets move on the curved screen to simulate the movement of the satellite. When the turntable adjusts its attitude to make the camera scan the targets, the relevant attitude data will be recorded. It should be noted that we pay more attention to the attitude adaptability of the satellite bus, and we make sure that all the targets are within the observing area in this scenario, so that most attitude data can be collected.

Before the satellite simulation bus scans along the trace, it first points to the target point 1, then gradually sweeps along the target distribution, and finally passes the target point 8. The attitude angles, bus angular velocities, and accelerations of the process are as shown in Table 3. As was mentioned above, when the attitude-controlling bus is working, the pitch angle is always maintained as 0, and the roll adjustment is first performed to make the imaging path intersect the targets trace, and then the yaw angle and the roll angular velocity are applied to make the composite velocity along the trace of targets.

The attitude angle and the angular velocity during the imaging process are shown in Figs. 14, 15, respectively. In this case, the pitch angle does not affect the bus attitude, and the roll angle contributes more than the yaw angle does when the simulation platform adapts the attitude. To make the graph more intuitive, the triaxial attitude angular velocities are separated and shown in Fig. 15(a) and (b). It can be seen that the roll angular velocity still takes the dominance, which means that much more attention should be paid

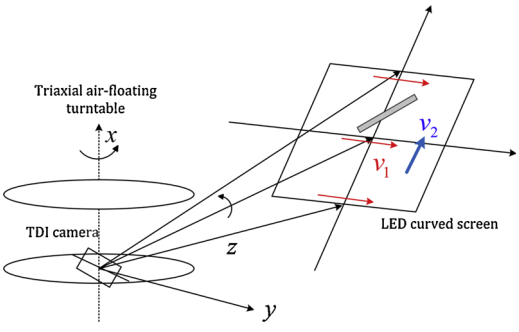

Fig. 13. Sketch map of Smart Imaging simulation.

Table 2
Location of the Target points.

Target point	Latitude(°)	Longitude(°)
1	−16.274	96.112
2	−16.654	96.801
3	−17.051	97.579
4	−18.150	98.746
5	−18.650	99.866
6	−19.122	100.974
7	−19.537	102.006
8	−19.860	103.322

Table 3
Attitude data of Smart Imaging simulation.

	Target point	Satellite nadir point	Time						
	(Lat,Lon)(°)	(Lat,Lon)(°)	1 Dec 2018	ψ (°)	φ (°)	$\dot{\psi}$ (°/s)	$\dot{\varphi}$ (°/s)	$\ddot{\psi}$ (°/s^2)	$\ddot{\varphi}$ (°/s^2)
1	(-16.274,96.112)	(4.420,103.544)	04:29:5.360	−67.8931	−53.497	-	-	-	-
2	(-16.654,96.801)	(-10.779,100.360)	04:29:44.648	−67.7631	−46.644	0.0033	0.1744	-	-
3	(-17.051,97.579)	(-13.417,99.793)	04:30:27.998	−67.6431	−34.312	0.0028	0.2845	-1.2474×10^{-5}	0.0025
4	(-18.150,98.746)	(-18.129,98.758)	04:31:45.506	−67.5931	−0.23	0.0006	0.4397	-2.7392×10^{-5}	0.0020
5	(-18.650,99.866)	(-21.768,97.932)	04:32:45.422	−67.6822	30.458	−0.0015	0.5122	-3.5586×10^{-5}	0.0012
6	(-19.122,100.974)	(-25.337,97.092)	04:33:44.265	−67.7311	47.922	−0.0008	0.2968	1.1149×10^{-5}	−0.0037
7	(-19.537,102.006)	(-28.642,96.281)	04:34:38.806	−67.7921	56.256	−0.0011	0.1528	-5.2694×10^{-5}	−0.0026
8	(-19.860,103.322)	(-2.583,102.085)	04:35:43.780	−67.8831	61.4517	−0.0014	0.0800	-4.34223×10^{-5}	−0.0011

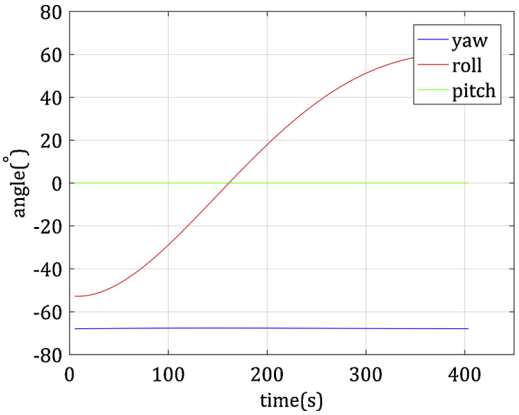

Fig. 14. Attitude angle of scanning along the trace of targets.

to the roll attitude when considering the maneuverability of the satellite bus. Usually, the angular velocity is no more than when the satellite bus is in the process of maneuvering [17,18].

The attitude angular accelerations are also shown in Fig. 16. The roll angular acceleration in Fig. 16(a) reaches a maximum of $0.0077^{\circ}/s^2$ and the minimum of yaw angular acceleration in Fig. 16(b) is $-5.2285 \times 10^{-5^{\circ}}/s^2$. The roll acceleration is still our focus. In practical use, the limit of angular acceleration should be $0.5^{\circ}/s^2$, although the value sometimes depends on the maneuverability of the flywheel [17,18]. From Table 3 and Fig. 16, we can see the roll angular acceleration easily meets the basic requirement, which means our method demands little for the maneuverability of the satellite bus.

5.3. On-orbit verification of Smart Imaging method

The imaging technology proposed in this paper, which is also called Smart Imaging, owns the advantage of high spatiotemporal resolution, and shows outstanding application prospects such as emergent disaster forecasting and rare resource exploring. In 2015, Changchun Institute of Optics, Fine Mechanics and Physics, Chinese Academy of Sciences launched the JL-1 Smart Verication Satellite which was specially designed to verify this technology on orbit. As shown in Fig. 17, it is a certain region of Atlanta, USA, which is scanned by the Smart Verication Satellite. The angle between the sub-satellite point trajectory and imaging path is 1/5 ~ 1/4 of our Smart Image mode's coverage. For the conventional method, if the whole area in the scene is to be covered, the imaging time will be greatly extended considering the revisit period of the satellite. The Smart Imaging technique is especially suitable for

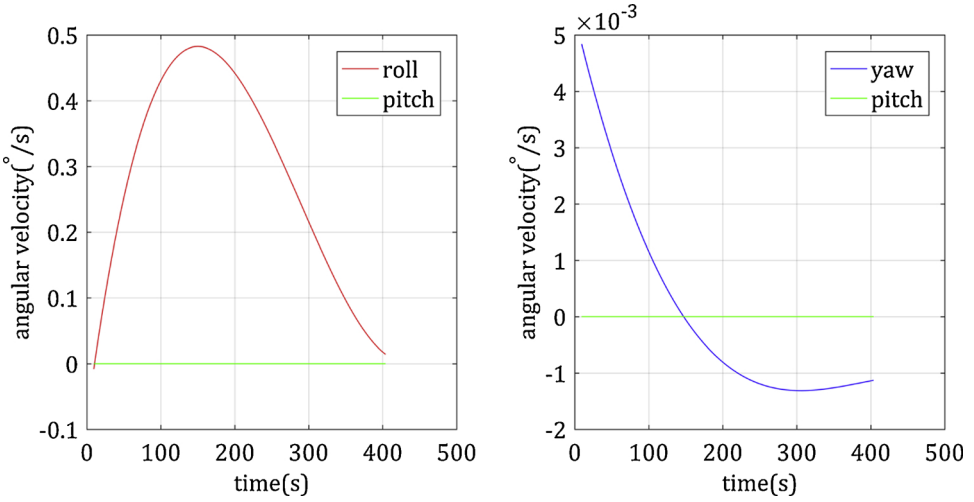

Fig. 15. Attitude angular velocity of scanning along the trace of targets. (a) Roll and pitch angular velocity. (b) Yaw and pitch angular velocity.

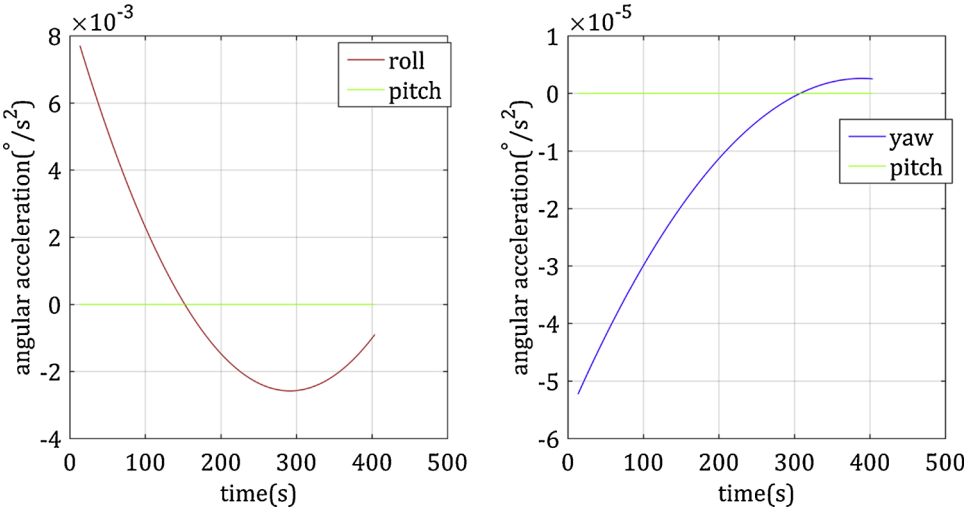

Fig. 16. Attitude angular acceleration of scanning along the trace of targets. (a) Roll and pitch angular acceleration. (b) Yaw and pitch angular acceleration.

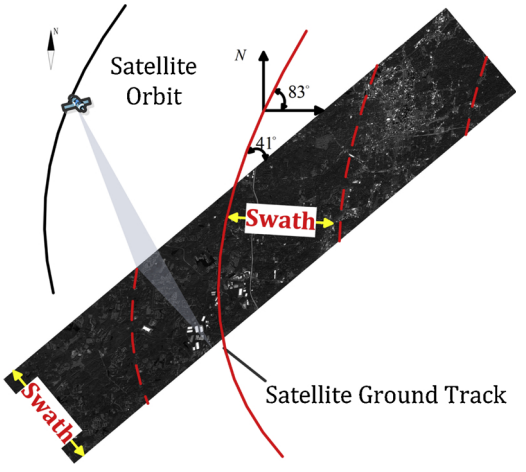

Fig. 17. Region of Atlanta obtained by Smart Imaging.

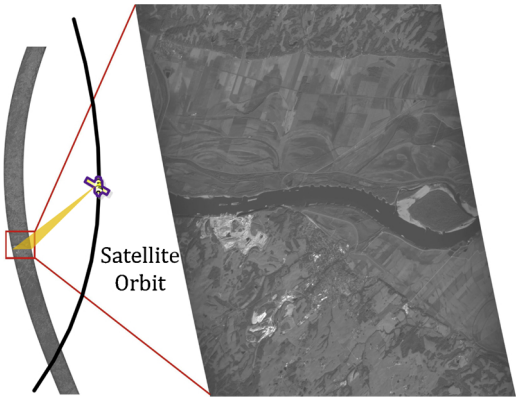

Fig. 18. Region of Mississippi River obtained by Smart Imaging.

observing tasks with the target area deviant from the satellite track, which can greatly improve the scanning efficiency.

Another successful example is shown in Fig. 18. It is a certain area of the Mississippi River in the United States. When the satellite is orbiting, the satellite boresight is pointing to the curve-distributed targets by real-time attitude adjustment. It can also be seen from the partial enlarged diagram that the image is of good quality and the texture details are quite clear.

6. Conclusion

In this paper, we propose a dynamic push-broom imaging method for the curve-distributed targets. Firstly, a new coverage algorithm is devised which maximizes the number of detectable targets by three-dimensional spatial vascular cube. Then a triaxial attitude model is built to extract the attitude parameters and make the satellite bus adapt its attitude to scan along the trace of targets. In the simulation experiment, the Yangtze River Delta is taken as an example to evaluate the coverage algorithm; a ground simulation is also performed to test the attitude adaptation of the satellite. Finally, JL-1 Smart Verification Satellite scanned a region of Atlanta. The imaging temporal resolution is improved by more than 4 times compared with traditional pushbroom pattern. Another example of the Mississippi River also showed great performance. The correctness of our method of dynamic push-broom imaging along the trace of targets is verified.

In some scenarios, certain targets are of more importance, which should be given higher priority. In the perspective of fitting algorithm, the coordinates of these targets are ought to be assigned larger weight to make sure they are collected by the sensor, for example, Weighted Least Squares. Under this circumstance, some constraints need to be considered to ensure the higher priority targets are collected when fitting the trace, for instance, the number of the higher priority targets, the relative position between these targets and the satellite track, and the attitude maneuverability of the satellite. This part would be covered in the future work.

Currently, there is an increasing number of manmade satellites sent into the space, which need to be carefully monitored. Considering the disturbance of the atmosphere, it will be a better choice to observe them from the outer space. Apart from the ground targets, our method might also be applied to these space-based objects. In this case, the boresight of the satellite does not point to the ground, but to the space. This might also be the possible extended research or application of this paper.

Acknowledgements

The work was partly supported by the National Natural Science Foundation of China (NSFC) under project No. 61705222.

References

[1] D. Habet, M. Vasquez, Y. Vimont, Bounding the optimum for the problem of scheduling the photographs of an agile earth observing satellite, Computational Optimization and Applications 47 (2) (2010) 307–333 10.1007/s10589-008-9220-7. //WOS:000281698100006.

[2] J.R. Irons, J.L. Dwyer, J.A. Barsi, The next landsat satellite: The landsat data continuity mission, Remote Sensing of Environment 122 (2012) 11–21, https://doi.org/10.1016/j.rse.2011.08.026 //WOS:000308680600003.

[3] J. Bingqiang, Y. Dong, S. Zhaowei, Trajectory optimization for satellite fast attitude maneuver based on collocation method, 2014 International Conference on Mechatronics and Control (ICMC), IEEE (2014) 1294–1298, https://doi.org/10.1109/ICMC.2014.7231761.

[4] R. Xu, H. Chen, X. Liang, H. Wang, Priority-based constructive algorithms for scheduling agile earth observation satellites with total priority maximization, Expert Systems with Applications 51 (2016) 195–206, https://doi.org/10.1016/j.eswa.2015.12.039 //WOS:000370899300017.

[5] P. Tangpattanakul, N. Jozefowiez, P. Lopez, A multi-objective local search heuristic for scheduling earth observations taken by an agile satellite, European Journal of Operational Research 245 (2) (2015) 542–554, https://doi.org/10.1016/j.ejor.2015.03.011 //WOS:000355360900018.

[6] E. Bensana, G. Verfaillie, J. Agnese, N. Bataille, D. Blumstein, Exact and inexact methods for daily management of earth observation satellite, Space Mission Operations and Ground Data Systems-SpaceOps' 96, (1996), p. 507.

[7] N. Bianchessi, J.-F. Cordeau, J. Desrosiers, G. Laporte, V. Raymond, A heuristic for the multi-satellite, multi-orbit and multi-user management of earth observation satellites, European Journal of Operational Research 177 (2) (2007) 750–762, https://doi.org/10.1016/j.ejor.2005.12.026 //WOS:000242302200007.

[8] W.J. Wolfe, S.E. Sorensen, Three scheduling algorithms applied to the earth observing systems domain, Management Science 46 (1) (2000) 148–166 10.1287/mnsc.46.1.148.15134. //WOS:000085645700012.

[9] J. Li, F. Yao, B. Bai, R. He, A decomposition-based algorithm for imaging satellites scheduling problem, International Conference on Information Engineering and Computer Science, IEEE (2009) 1–6.
[10] T. Kouyama, A. Kanemura, S. Kato, N. Imamoglu, T. Fukuhara, R. Nakamura, Satellite attitude determination and map projection based on robust image matching, Remote Sensing 9 (1) (2017) 90, https://doi.org/10.3390/rs9010090.
[11] R. Sugimoto, T. Kouyama, A. Kanemura, S. Kato, N. Imamoglu, R. Nakamura, Automated attitude determination for pushbroom sensors based on robust image matching, Remote Sensing 10 (10) (2018) 1629, https://doi.org/10.3390/rs10101629.
[12] J. Wang, P. Yu, C. Yan, J. Ren, B. He, Space optical remote sensor image motion velocity vector computational modeling, error budget and synthesis, Chinese Optics Letters 3 (7) (2005) 414–417 //CSCD:2210077.
[13] J.R. Wertz, Spacecraft attitude determination and control, Springer Science and Business Media, 2012.
[14] R. Zhang, Dynamics and control of satellite orbit and attitude, Beijing University of Aerospace Astronautics Press, 1998.
[15] J.A. Shen, G.J. Zhang, X.G. Wei, Simulation analysis of dynamic working performance for star trackers, Journal of the Optical Society of America a-Optics Image Science and Vision 27 (12) (2010) 2638–2647, https://doi.org/10.1364/josaa.27.002638.
[16] S. Zhang, F. Xing, T. Sun, Z. You, M.S. Wei, Novel approach to improve the attitude update rate of a star tracker, Optics Express 26 (5) (2018) 5164–5181, https://doi.org/10.1364/oe.26.005164 //WOS:000427147200008.
[17] B. Wie, J.B. Lu, Feedback-control logic for spacecraft eigenaxis rotations under slew rate and control constraints, Journal of Guidance Control and Dynamics 18 (6) (1995) 1372–1379, https://doi.org/10.2514/3.21555 //WOS:A1995TE75800022.
[18] B. Wie, D. Bailey, C. Heiberg, Rapid multitarget acquisition and pointing control of agile spacecraft, Journal of Guidance Control and Dynamics 25 (1) (2002) 96–104, https://doi.org/10.2514/2.4854 //WOS:000173405800012.